Electronic Supplementary Information

Determining a membrane's shear modulus, independent of its area-dilatation modulus, *via* capsule flow in a converging micro-capillary

P. Dimitrakopoulos* and S. Kuriakose

Department of Chemical and Biomolecular Engineering,

University of Maryland, College Park, Maryland 20742, USA

(Dated: February 2, 2015)

* dimitrak@umd.edu

1. MATHEMATICAL FORMULATION AND COMPUTATIONAL ALGORITHM

A. Fluid and Membrane Dynamics

We consider a three-dimensional capsule (i.e. a fluid volume enclosed by a thin elastic membrane) with a spherical undisturbed shape. The capsule is flowing along the centerline of a straight micro-channel with a converging section in the middle connecting two square channels, as shown in figure 1. We emphasize that the centerline requirement is not a restriction for our study since this is the steady-state location of spherical capsules in a square channel [5]; thus our capsules are expected to have been aligned with the micro-capillary centerline during their motion in the area further upstream the constriction.

To facilitate our description, we imagine that the channel is horizontal as illustrated in figure 1(a). Thus, the flow direction (i.e. the x-axis) corresponds to the channel's or capsule's length, the z-direction will be referred as height while the y-direction will be referred as width. The height of the square micro-channel at the left is $3\ell_z$ and that of the square micro-channel at the right $2\ell_z$. The converging middle section, which connects the two square micro-channels, has length $\ell_{con} = \ell_z$. Each of the two square micro-channels has length $12\ell_z$, and thus the length of the entire microfluidic device is $25\ell_z$. The half-height ℓ_z of the downstream square micro-channel serves as the length scale for the present problem while the origin of the co-ordinate system is placed at the beginning of this channel (just after the converging middle section) as shown in figure 1(a).

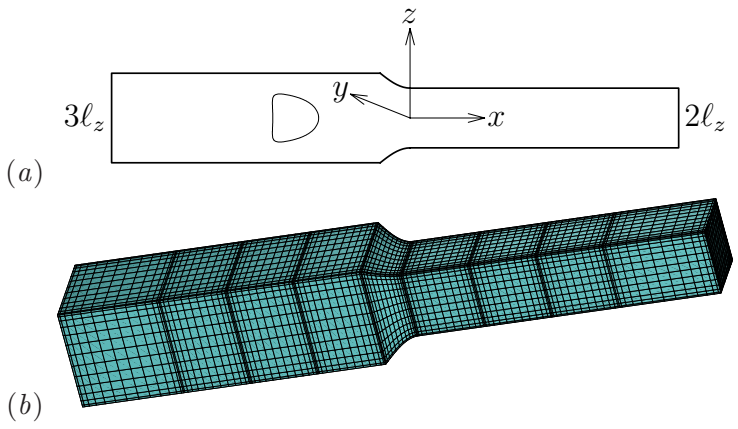

FIG. 1. (a) Illustration of an elastic capsule flowing at the centerline of a converging square micro-channel. (b) Spectral boundary element discretization of the microfluidic geometry.

The shape of the converging middle section in our micro-geometry is defined by a "quarter-cosine" variation, which for the co-ordinate system shown in figure $1(a)$ is given by

$$f(x) = \ell_z \Big\{ \frac{3}{2} + \frac{1}{2} \cos \Big[(\frac{x}{\ell_z} + 2) \frac{\pi}{2} \Big] \Big\} \tag{1}$$

where $-1 \leq x/\ell_z \leq 0$ and $f(x)$ defines the geometry's height $z(x)$ or width $y(x)$. It is of interest to mention that, although the results presented in this paper were derived utilizing this shape of the converging middle section, we derived very similar (or practically identical) results utilizing other converging shapes, including "half-cosine" variation

$$f(x) = \ell_z \Big\{ \frac{5}{4} + \frac{1}{4} \cos \Big[(\frac{x}{\ell_z} - 1) \pi \Big] \Big\} \tag{2}$$

and "straight-line" connection

$$f(x) = \ell_z \Big(1 - \frac{1}{2} \frac{x}{\ell_z} \Big) \tag{3}$$

The capsule's interior and exterior are Newtonian fluids, with viscosities $\lambda\mu$ and μ, and the same density. The capsule size a is specified by its volume $V = 4\pi a^3/3$ and is comparable to the micro-geometry's half-height ℓ_z. In addition, we consider that the capsule is slightly over-inflated, made of a strain-hardening membrane following the Skalak *et al.* constitutive law [10] (and thus called Skalak capsule in this paper) with comparable shearing and area-dilatation resistance. This capsule description represents well bioartificial capsules such as the capsules made of covalently linked human serum albumin (HSA) and alginate used in the experimental study of Risso, Collé-Pailot and Zagzoule [9].

At time $t = 0$ the capsule is located at $-5\ell_z$ on the micro-channel centerline, the flow is turn on inside the microfluidic device and we investigate the transient dynamics of the capsule as it enters and exits the constriction which occupies the x-region $[-\ell_z, 0]$. (The specific choice for the capsule's initial position does not affect the capsule deformation and motion inside the constriction or downstream of it, i.e. we obtained identical results even for capsules placed further upstream the constriction.)

At the micro-capillary ends the flow approaches the undisturbed flow $\boldsymbol{u}^\infty = (u_x^\infty, 0, 0)$ in a square channel which serves as the boundary condition assuming a fixed flow rate Q inside the micro-device. For the downstream square micro-channel with half-height ℓ_z and half-width $\ell_y = \ell_z$, this velocity is given by

$$\frac{u_x^\infty}{\Upsilon} = (\ell_z^2 - z^2) + \sum_{m=1}^{\infty} B_m \cosh(\frac{b_m y}{\ell_z}) \cos(\frac{b_m z}{\ell_z}) \tag{4}$$

where

$$\Upsilon = -\frac{1}{2\mu}\frac{\mathrm{d}p}{\mathrm{d}x}, \qquad b_m = \frac{(2m-1)\pi}{2} \qquad \text{and} \qquad B_m = \frac{(-1)^m\, 4\,\ell_z^2}{b_m^3 \cosh(\frac{b_m \ell_y}{\ell_z})} \tag{5}$$

while p is the dynamic pressure [5]. By integrating over the channel's cross-section, we can easily show that the volumetric flow rate Q is given by

$$\frac{Q}{\Upsilon} = \frac{8\,\ell_y\,\ell_z^3}{3} + \sum_{m=1}^{\infty} B_m (\frac{2\ell_z}{b_m})^2 \sinh(\frac{b_m \ell_y}{\ell_z}) \sin(b_m) \tag{6}$$

The average velocity is $\mathcal{U} = Q/(\ell_y \ell_z)$ while the maximum undisturbed velocity at the centerline of the square channel is $\mathcal{U}_{max}/\mathcal{U} \approx 2.096$. In our computations, we truncated the infinite (convergent) series associated with the channel's undisturbed flow when $m = 40$. We note that for the upstream square micro-channel the half-height is $1.5\ell_z$ and the average velocity is $4/9\,\mathcal{U}$.

Assuming low-Reynolds-number flows, the governing equations in fluid 2 are the Stokes equations and continuity,

$$\nabla \cdot \boldsymbol{\sigma} \equiv -\nabla p + \mu \nabla^2 \boldsymbol{u} = 0 \quad \text{and} \quad \nabla \cdot \boldsymbol{u} = 0 \tag{7}$$

where $\boldsymbol{\sigma}$ is the stress tensor and $\boldsymbol{u}$ the fluid velocity. Inside the capsule, the same equations apply with the viscosity replaced by $\lambda\mu$. It is of interest to note that in small length-scale systems, such as microfluidic channels, low-Reynolds-number flows are easily achievable [5, 11]. (For example, in a microfluidic channel with size $\ell_y = 100\,\mu m$, the Reynolds number remains $Re = O(10^{-3})$ even for velocities up to $\mathcal{U} = 10\,mm/s$ when we consider the density and viscosity of water.)

For the current problem, the system surface S_B consists of the capsule interface S_c, the micro-device's solid surface S_s, and the fluid surface S_f of the inlet and outlet of the micro-device. At the capsule's interface, the velocity is continuous and we define the surface stress vector (or hydrostatic traction) $\Delta \boldsymbol{f}$ from the stress tensor $\boldsymbol{\sigma}$ and the surface unit normal $\boldsymbol{n}$, i.e.

$$\boldsymbol{u}_1 = \boldsymbol{u}_2 = \boldsymbol{u} \quad \text{and} \quad \Delta \boldsymbol{f} \equiv \boldsymbol{n} \cdot (\boldsymbol{\sigma}_2 - \boldsymbol{\sigma}_1) \tag{8}$$

Here the subscripts designate quantities evaluated in fluids 1 and 2, respectively, while $\boldsymbol{n}$ is the unit normal which we choose to point into fluid 2. The boundary conditions on the rest surfaces are

$$\boldsymbol{u} = 0 \quad \text{on the solid boundary } S_s \tag{9}$$

$$\boldsymbol{u} = \boldsymbol{u}^{\infty} \quad \text{on the fluid boundary } S_f \tag{10}$$

Based on standard boundary integral formulation, the velocity at a point $\boldsymbol{x}_0$ on the system surface S_B may be expressed as a surface integral of the force vector $\boldsymbol{f} = \boldsymbol{n} \cdot \boldsymbol{\sigma}$ and the velocity $\boldsymbol{u}$ over all points $\boldsymbol{x}$ on the boundary S_B,

$$\begin{aligned} \Omega\, \boldsymbol{u}(\boldsymbol{x}_0) =& -\int_{S_c} \left[\boldsymbol{S} \cdot \Delta \boldsymbol{f} - \mu(1-\lambda)\, \boldsymbol{T} \cdot \boldsymbol{u} \cdot \boldsymbol{n}\right](\boldsymbol{x})\, \mathrm{d}S \\ & - \int_{S_s \cup S_f} \left(\boldsymbol{S} \cdot \boldsymbol{f} - \mu\, \boldsymbol{T} \cdot \boldsymbol{u} \cdot \boldsymbol{n}\right)(\boldsymbol{x})\, \mathrm{d}S \end{aligned} \tag{11}$$

where the coefficient Ω takes values $4\pi\mu(1+\lambda)$ and $4\pi\mu$ for points $\boldsymbol{x}_0$ on the surfaces S_c and $S_s \cup S_f$ respectively. The tensors $\boldsymbol{S}$ and $\boldsymbol{T}$ are the fundamental solutions for the velocity and stress for the three-dimensional Stokes equations, i.e. known functions of the system surface S_B [1, 2, 14]

Owing to the no-slip condition at the interface, the time evolution of the material points of the membrane may be determined via the kinematic condition at the interface

$$\frac{\partial \boldsymbol{x}}{\partial t} = \boldsymbol{u} \tag{12}$$

To produce a closed system of equations, the surface stress $\Delta \boldsymbol{f}$ on the capsule interface is determined by the membrane dynamics. Our membrane description is based on the well-established continuum approach and the theory of thin shells by considering the membrane as a two-dimensional continuum with shearing and area-dilatation resistance but negligible bending resistance. This modeling has been proven to be an excellent description of a wide range of thin elastic membranes (such as biocompatible alginate, synthetic polysiloxane and aminomethacrylate capsules) whose thickness is several orders of magnitude smaller than the size of the capsules (up to a membrane thickness of 5% the capsule size), and their bending resistance is very small compared to their shearing resistance [3, 4, 8].

The surface stress is determined by the in-plane stresses

$$\Delta \boldsymbol{f} = -\nabla_s \cdot \boldsymbol{\tau} = -(\tau^{\alpha\beta}|_{\alpha}\, \boldsymbol{t}_{\beta} + b_{\alpha\beta}\, \tau^{\alpha\beta}\, \boldsymbol{n}) \tag{13}$$

where the Greek indices range over 1 and 2, while Einstein notation is employed for (every two) repeated indices. In this equation, the $\tau^{\alpha\beta}|_{\alpha}$ notation denotes covariant differentiation, $\boldsymbol{t}_{\beta} = \partial \boldsymbol{x}/\partial \theta^{\beta}$ are the tangent vectors on the capsule surface described with arbitrary curvilinear coordinates θ^{β}, and $b_{\alpha\beta}$ is the surface curvature tensor [4, 8]. The in-plane stress

tensor $\boldsymbol{\tau}$ is described by the strain-hardening constitutive law of Skalak *et al.* [10] which relates $\boldsymbol{\tau}$'s eigenvalues (or principal elastic tensions $\tau_\beta^P, \beta = 1, 2$) with the principal stretch ratios λ_β by

$$\tau_1^P = \frac{G_s \lambda_1}{\lambda_2} \{\lambda_1^2 - 1 + C\lambda_2^2[(\lambda_1\lambda_2)^2 - 1]\} \tag{14}$$

Note that the reference shape of the elastic tensions is the spherical quiescent shape of the capsule while to calculate τ_2^P reverse the λ_β subscripts. In Eq.(14), G_s is the membrane's shear modulus while the dimensionless parameter C describes the membrane hardness (i.e. the strength of its strain-hardening nature) and is associated with the scaled area-dilatation modulus G_a of the membrane, $G_a/G_s = 1 + 2C$ [8, 10].

We further consider that the capsule is subjected to a positive osmotic pressure difference between the interior and exterior fluids, i.e. the capsule is (slightly) over-inflated and thus prestressed. Such consideration is motivated by the fact that, owing to osmotic effects during their fabrication, artificial capsules are often slightly over-inflated as the bioartificial capsules used in the experimental investigation of Risso, Collé-Pailot and Zagzoule [9].

To quantify the capsule over-inflation, we define the prestress parameter α_p such that all lengths in the undeformed capsule would be scaled by $(1 + \alpha_p)$ relatively to the reference shape [5–7]. Since the capsule is initially spherical, its membrane is initially prestressed by an isotropic elastic tension $\tau_0 = \tau_\beta^P(t = 0)$ which depends on the employed constitutive law and its parameters but not on the capsule size. For example, for a Skalak capsule with $C = 1$ and $\alpha_p = 0.05$, the undisturbed capsule radius a is 5% higher than that of the reference shape and the initial membrane tension owing to prestress is $\tau_0/G_s \approx 0.3401$. removes the buckling instability observed in axisymmetric-like flows. (See section 2 in Ref.[5].)

B. Definition of Geometric and Physical Variables

To describe the capsule deformation, we determine the capsule projection lengths along the three axes, L_x, L_y and L_z, as the maximum distance in the x, y and z coordinates of the capsule surface. For a given capsule shape, we determine accurately these three capsule dimensions by employing a Newton method to solve the optimization problems using the spectral discretization points on the membrane. Our results are expressed as functions of the capsule's centroid $\boldsymbol{x}_c = (x_c, y_c, z_c)$ where $y_c = z_c = 0$ for this problem owing to the centerline motion.

In this study, we assume that the flow rate Q inside the channel is fixed. Thus we apply velocity boundary conditions at the channel's inlet and outlet (see Eq.(8)) and we solve for the fluid force at the channel ends. The fluid pressure at the channel's inlet and outlet, P_{in} and P_{out}, is determined as the surface-average of the normal force on these two surfaces

$$P_{in} = \frac{\int_{in} f_x \, \mathrm{d}S}{\int_{in} \mathrm{d}S} \qquad \text{and} \qquad P_{out} = -\frac{\int_{out} f_x \, \mathrm{d}S}{\int_{out} \mathrm{d}S} \tag{15}$$

(Note that although we have chosen this way to determine the pressure at the channel ends, our computational results show that the fluid normal force, or pressure, at each channel end is constant to at least 4 significant digits among the spectral discretization points.) The pressure difference at the channel ends is $\Delta P = P_{in} - P_{out}$ and we also calculate the additional pressure difference owing to the presence of the capsule in the channel,

$$\Delta P^{+} = \Delta P - \Delta P^{nc} \tag{16}$$

where ΔP^{nc} is the pressure difference at the channel ends when no capsule is present in the channel. As the capsule moves in the channel, its volume-average velocity is determined from surface properties, i.e.

$$\boldsymbol{U} = \frac{1}{V} \int_V \boldsymbol{u} \, \mathrm{d}V = \frac{1}{V} \int_{S_c} (\boldsymbol{n} \cdot \boldsymbol{u}) \, \boldsymbol{x} \, \mathrm{d}S \tag{17}$$

In our work, we consider Skalak capsules with different size a/ℓ_z, membrane hardness C and prestress α_p. The present problem depends on two additional dimensionless parameters, the fluids viscosity ratio λ and the capillary number Ca defined as

$$\mathrm{Ca} = \frac{\mu \mathcal{U}}{G_s} \tag{18}$$

where $\mathcal{U}$ is the average undisturbed velocity at the downstream square micro-channel. It is of interest to note that the capillary number, as defined by Eq.(18), does not contain any length scale, and thus it may be considered as a dimensionless flow rate. In our study, the velocity is scaled with the average undisturbed velocity $\mathcal{U}$ and the pressure with the associated pressure scale, $\Pi = \mu \mathcal{U}/(2\ell_z)$, in the downstream square channel.

C. Membrane Spectral Boundary Element Algorithm

The numerical solution of the boundary integral equation, (11), is achieved through our spectral boundary element method for membranes [4, 5]. Briefly, each boundary is divided

into a moderate number N_E of surface elements which are parameterized by two variables ξ and η on the square interval $[-1,1]^2$. The geometry and physical variables are discretized using Lagrangian interpolation in terms of these parametric variables. The N_B basis points (ξ_i, η_i) for the interpolation are chosen as the zeros of orthogonal polynomials of Gauss-type. This is equivalent to an orthogonal polynomial expansion and yields the spectral convergence associated with such expansions.

The boundary integral equation (11) admits two different types of points. The collocation points $\boldsymbol{x}_0$ where the equation is required to hold and the basis points $\boldsymbol{x}$ where the physical variables $\boldsymbol{u}$ and $\boldsymbol{f}$ are specified or determined. Our spectral boundary element method employs collocation points $\boldsymbol{x}_0$ of Legendre–Gauss quadrature, i.e. in the interior of the elements. As a result the boundary integral equation holds even for singular elements, i.e. the elements which contain the corners of the channel geometry. (Similar approach has been utilized in our earlier papers for droplets attached to solid surfaces, and vascular endothelial cells or leukocytes adhering to the surface of blood vessels, e.g. [1, 12, 13].) In addition, we use basis points $\boldsymbol{x}$ of Legendre–Gauss–Lobatto quadrature and thus the physical variables are determined in the interior and on the edges of the spectral elements. For the time integration, we employed the 2nd-order Runge-Kutta scheme with a typical time step $\Delta t = 0.5 \times 10^{-3}$. Further details on our spectral boundary element algorithms are given in our earlier publications, i.e. [2, 4, 5, 14].

Three-dimensional views of the problem geometry are shown in figure $1(b)$. In the present paper, the majority of computations were performed with a discretization employing $N_E = 44$ elements. The capsule surface is divided into 6 elements, while we define 9 rows of 4 elements each on the micro-device's solid surface and 1 spectral element for the inlet and outlet of the device, as seen in figure $1(b)$.

In our work we utilized $N_B = 14$–16 basis points; in the paper we present our results for $N_B = 14$ and use those with denser grids as convergence runs. In particular, to verify the accuracy of our results, we performed convergence runs covering the entire interfacial evolution for several capsules and flow rates. Our convergence runs showed that our results for the interfacial shape, the capsule velocity and the additional pressure difference presented in this work were determined with an accuracy of at least 3 significant digits.

The problem studied in this paper admits three independent symmetry planes, $y = 0$, $z = 0$ and $y = z$. Exploiting these symmetries reduces the memory requirements for the

storage of the system matrices by a factor of 8^2, the computational time for calculating the system matrices by a factor of 8 and the solution time of the linear systems via direct solvers by a factor of 8^3. Most of our computations were performed on multi-core computers utilizing the existing parallelization of our spectral boundary element algorithm via OpenMP directives for the calculation of the system matrices, and highly optimized, parallelized routines from the LAPACK library for the solution of the dense system matrices.

---

[1] P. Dimitrakopoulos and J. J. L. Higdon, On the displacement of three-dimensional fluid droplets from solid surfaces in low-Reynolds-number shear flows. *J. Fluid Mech.* **377**, 189–222 (1998).

[2] P. Dimitrakopoulos, Interfacial dynamics in Stokes flow via a three-dimensional fully-implicit interfacial spectral boundary element algorithm. *J. Comp. Phys.* **225**, 408–426 (2007).

[3] P. Dimitrakopoulos, Effects of membrane hardness and scaling analysis for capsules in planar extensional flows. *J. Fluid Mech.* **745**, 487–508 (2014).

[4] W. R. Dodson III and P. Dimitrakopoulos, Dynamics of strain-hardening and strain-softening capsules in strong planar extensional flows via an interfacial spectral boundary element algorithm for elastic membranes. *J. Fluid Mech.* **641**, 263–296 (2009).

[5] S. Kuriakose and P. Dimitrakopoulos, Motion of an elastic capsule in a square microfluidic channel. *Phys. Rev. E.* **84** 011906 (2011).

[6] S. Kuriakose and P. Dimitrakopoulos, Deformation of an elastic capsule in a rectangular microfluidic channel. *Soft Matter*, **9** 4284–4296 (2013).

[7] S.-Y. Park and P. Dimitrakopoulos Transient dynamics of an elastic capsule in a microfluidic constriction. *Soft Matter* **9**, 8844–8855 (2013).

[8] C. Pozrikidis (ed.), *Modeling and Simulation of Capsules and Biological Cells*. Chapman and Hall, London (2003).

[9] F. Risso, F. Collé-Pailot and M. Zagzoule, Experimental investigation of a bioartificial capsule flowing in a narrow tube. *J. Fluid Mech.* **547**, 149–173 (2006).

[10] R. Skalak, A. Tozeren, R. P. Zarda, and S. Chien, Strain energy function of red blood cell membranes. *Biophys. J.* **13**, 245–264 (1973).

[11] S.-Y. Teh, R. Lin, L.-H. Hung and A. P. Lee, Droplet microfluidics. *Lab Chip* **8**, 198–220

(2008).

[12] Y. Wang and P. Dimitrakopoulos, Normal force exerted on vascular endothelial cells. *Phys. Rev. Lett.* **96**, 028106(1-4) (2006).

[13] Y. Wang and P. Dimitrakopoulos, Nature of the hemodynamic forces exerted on vascular endothelial cells or leukocytes adhering to the surface of blood vessels. *Phys. Fluids* **18**, 087107(1-14) (2006).

[14] Y. Wang and P. Dimitrakopoulos, A three-dimensional spectral boundary element algorithm for interfacial dynamics in Stokes flow. *Phys. Fluids* **18**, 082106(1-16) (2006).